

4. COLOR REFLECTANCE SPECTROSCOPY: A TOOL FOR RAPID CHARACTERIZATION OF DEEP-SEA SEDIMENTS¹

A. C. Mix,² W. Rugh,² N. G. Pisias,² S. Veirs,³ Leg 138 Shipboard Sedimentologists (T. Hagelberg, S. Hovan, A. Kemp, M. Leinen, M. Levitan, and C. Ravelo),⁴ and the Leg 138 Scientific Party⁴

INTRODUCTION

During ODP Leg 138, we tested a prototype instrument, developed at Oregon State University, for measuring light reflectance in 511 channels of the visible and near-infrared bands. The technique of reflectance spectroscopy has been used for some time in chemistry and mineralogy (e.g., Hunt, 1977; Gaffey, 1986) and has found applications in remote sensing of natural reflectance from aircraft and satellites (Hoffer, 1984; Goetz et al., 1982), but this technique has not yet been widely used in marine geology (e.g., Chester and Elderfield, 1966; Barranco et al., 1989). Our goal here is to assess the utility of reflectance spectroscopy as a rapid, nonintrusive tool for characterizing the lithology of deep-sea sediments. In this chapter, we report the instrumentation used for the first time during Leg 138, give a few examples of preliminary shipboard results, and make recommendations about further development of the technique in the context of ocean drilling. A more complete discussion of the scientific results appears elsewhere.

INSTRUMENTATION

The reflectance instrument used during Leg 138 consists of four subsystems: (1) a core transport, (2) illumination and sensing optics, (3) a spectrograph and detector, and (4) computer control and data processing (Fig. 1). Split sediment cores move under the sensing optics on a computer-controlled conveyor system. A regulated light source illuminates the sediment surface via a glass fiber-optic cable. The sensing head, which moves vertically to maintain a constant distance off the sediment surface, collects the reflected light. A second fiber-optic cable delivers the reflected light to the spectrograph, where it is split into its spectrum with a diffraction grating and detected in a 511-channel diode array. The measurement system is controlled by a 386-PC computer, but raw data are written directly to a more powerful Sun UNIX workstation. This computer converts these data to reflectance spectra and makes them available for immediate analysis.

Core Transport System

A conveyor system transports split sediment cores under a stationary illuminating and sensing system so that a depth sequence can be measured automatically. The core transport used here is similar to the ODP multisensor track (MST) aboard *JOIDES Resolution* (Bearman, 1990). This track system, available from Analytical Services Corporation, is built on a rigid aluminum frame. The sediment core is placed in a fiberglass "boat," which is pulled by a Kevlar chain driven by a stepper motor (Compumotor A-106). In the prototype instrument used

during Leg 138, an optical encoder was not available to verify movement of the core because of cost constraints. This was not a serious problem, because the high-torque stepper motor was reliable; however, ideally an encoder should be used. The stepper motor was controlled by a 386-PC computer with a custom interface. This prototype did not include the Indexer system that exists on the ODP-MST device, again because of cost constraints, but instead drove the stepper motor using low-level software.

Illumination and Sensing System

An ideal light source for reflectance spectroscopy should have high intensity, a broad spectrum across all wavelengths of interest, and absolutely constant output. No light source achieves all of these specifications. To approximate these conditions at reasonable cost, our light source was a 100-W tungsten filament in a halogen-filled quartz bulb (Oriel Corp. Model 77501 broad-band source). The power supply was regulated to provide constant voltage (12V DC). An iris diaphragm allowed for adjustment of light intensity without changing the color temperature of the lamp, and a manual shutter interrupted the light beam for background calibration. In theory, halogen lamps should have minimal variation in their color spectrum through their operating life. We found this to be true for some lamps, but others evolved gradually, generally giving lower output intensities (as low as 70% of their maximum) and a slightly redder spectrum before burning out. Some produced more output shortly before burning out (the "Supernova Effect"). Different bulbs varied in output intensity by as much as 50%. All of these source effects were corrected in the final percentage reflectance data, based on analysis of reference materials.

It is not practical to locate a light source directly adjacent to a sample, so light must be delivered through an optical system. The prototype instrument transmits the light through a 1-m-long glass-fiber optic bundle into a light-baffled sample chamber. Transmission efficiency of light through the glass fiber ranges between 52% and 58% in wavelengths from 500 to 1000 nm. This efficiency falls off to about 40% by 400 nm. We measured wavelengths from 450 to 950 nm. The uniform transmission of light through the fiber-optic cable in this range of wavelengths is ideal in this application. As with the source effects, transmission effects on the light spectrum were corrected in the percentage reflectance data.

All measurements were performed in a dark sample chamber, with an opening just larger than the sediment core and core boat. This dark chamber reduced background noise from ambient light. Inside the sample chamber, the fiber-optic cable of the light source was terminated by a collimating lens in the side of the sensing head (Fig. 2). After passing through this lens, the illuminating beam was directed to a beam splitter. This splitter allowed us to mount the input cable and collimating lens out of the path of the reflected beam, which eliminated lens retro-reflection (back reflection off the lens) from the measurements. Half of the light passed through the splitter and was dissipated in a conical light trap opposite the collimating lens. The other half was deflected 90° by the beam splitter toward the sample. The axis of the resulting incident beam is perpendicular to the sediment surface. Variations in the roughness of the surface caused some deviation from this ideal condition, but this

¹ Mayer, L., Pisias, N., Janecek, T., et al., 1992. *Proc. ODP, Init. Repts.*, 138: College Station, TX (Ocean Drilling Program).

² Oregon State University, Corvallis, OR 97331, U.S.A.

³ Stanford University, Stanford, CA 94305, U.S.A.

⁴ Leg 138 Shipboard Sedimentologists and Scientific Party are as given in list of participants preceding the contents.

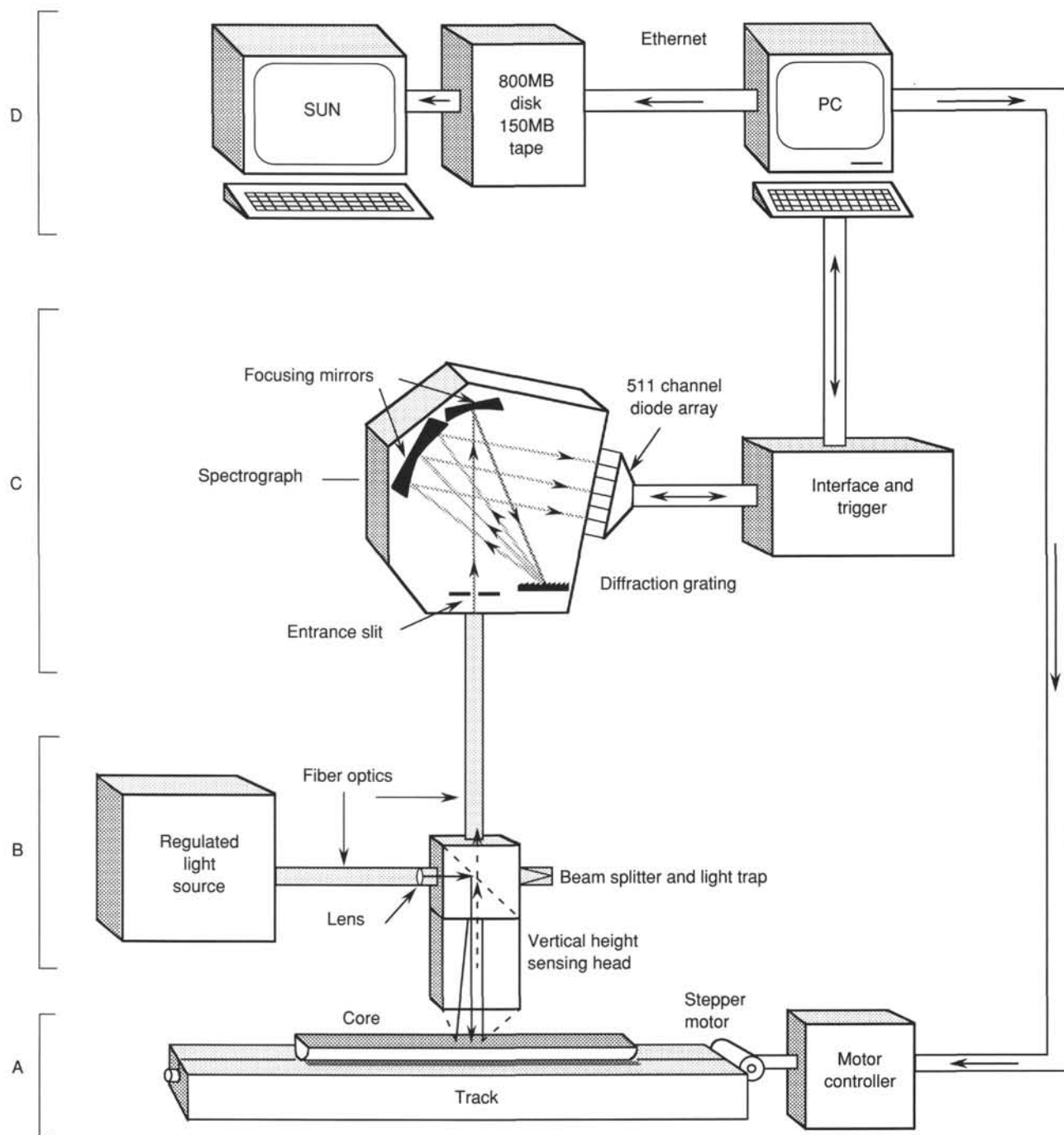


Figure 1. System overview. Four subsystems are shown (A) the core transport track, (B) light source and sensing optics, (C) the spectrograph and diode array detector, and (D) the computer control and data processing systems.

roughness was usually small enough that measurement quality was not affected significantly.

At the sediment surface, a 2-cm-diameter circular area was illuminated. We chose this spot size to avoid sensing the edges of the plastic core tube (about 6.6 cm inside diameter) and to allow us to measure temporal variability of lithology at reasonably close intervals, while providing smoothing on the scale of individual burrows (on the order of 1 cm, typically). In principle, an instrument could be designed having a variable illumination spot size to optimize measurement on a variety of scales for other applications.

The sensing head collected reflected light along an axis perpendicular to the sediment surface, similar to that of the incident beam.

Half the reflected beam passed through the beam splitter and entered another 1-m-long, fiber-optic cable, which delivered the reflected light beam to the spectrometer (Fig. 2).

We found it necessary to maintain a constant distance between the sediment surface and the sensing head to keep illumination intensity and collection geometry constant. With this instrument, the reflected beam intensity measured on reference materials was constant ($\pm 0.5\%$) over a ~1-cm range of core-to-sensor distance (roughly 10–11 cm distance from the measured surface to the beam splitter). Outside this constant intensity zone, the reflected beam intensity increased geometrically at distances less than 10 cm and decreased geometrically greater than 11 cm. To maintain constant distance from sample to

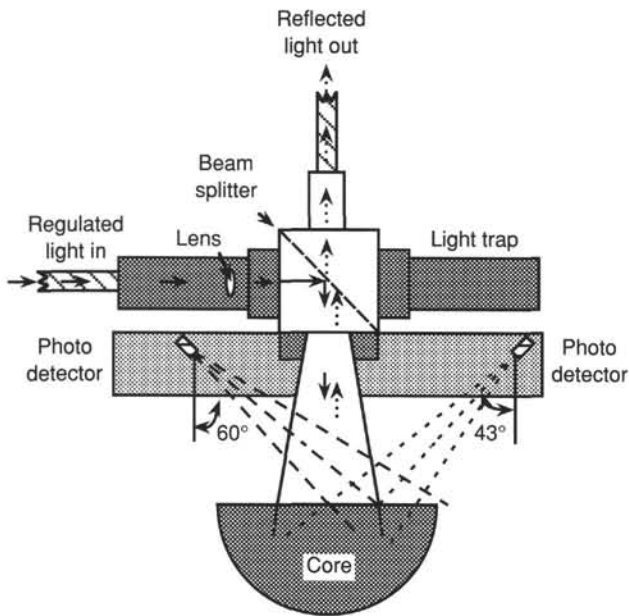


Figure 2. Schematic view of the sensing head optics. The collimated light beam enters from fiber optics at left and then is deflected down to the core (solid arrows). Reflected lights (dashed arrows) exit through fiber optics at top. The entire assembly is mounted on a motor-driven, rack-and-pinion vertical track to adjust core-to-sensor distance.

sensing head, two photodetectors were mounted diagonally on the sides of the sensing head (Fig. 2). Each measured one side of the reflected beam from different oblique angles (43° and 60° angles). Any deviations from the constant core-to-sensor distance resulted in differences in light intensity at the two photodetectors. A feedback error loop circuit detected these differences and transmitted this information to the 386-PC instrument control computer, which then calculated the sample-to-detector distance error and pulsed a DC servomotor to drive the sensor head up or down on a rack-and-pinion track. The length of the motor pulse was a function of the distance offset. The motor was pulsed, and distance was checked in a loop, until the desired sample-to-sensor distance was reached. This system maintained a constant distance within ± 0.4 mm. The reflectance error induced by this tolerance was insignificant for our purposes, $< 0.1\%$ on flat surfaces. Distance adjustment usually took about 1 s.

Spectrograph and Detector System

After the reflected light passed through the sensing head, the fiber-optic cable delivered it to the spectrograph—a 77400 Multispec (Oriel Corporation). Light entered this device (Fig. 1) through a 100-nm entrance slit. Slit width controls wavelength resolution at the detector, about 1.0 nm as configured here. A smaller slit would give finer resolution (unnecessary in this application) at the cost of a loss of beam intensity. A focusing mirror directed the light beam onto a diffraction grating. The grating used here had a blaze wavelength of 550 nm and a groove spacing of 400 lines/mm, yielding a spectrographic bandpass optimum of 530 nm. This diffraction grating spread the light beam across wavelengths from 400 to 1100 nm. A second focusing mirror directed this beam to the detector, with a flat focal field across a 25-mm beam width.

The wavelength-separated beam was detected by a 512-channel silicon photodiode array, which produced 511 channels of data, recording wavelengths 454 to 950 nm at 0.97-nm intervals. The detector was calibrated for wavelengths by measuring the output from a fluorescent light, which contained a narrow-band mercury emission line at 546.1 nm. A vernier adjustment rotated the diffraction grating

until this emission line was assigned to the correct wavelength in the detector. The fluorescent light was removed after calibration. After initial calibration, daily checks showed no drift in the position of this 546.1-nm line.

The advantage of a diode-array detector over the traditional motor-driven scanning monochromator and photomultiplier tube is that the entire spectrum can be collected rapidly (milliseconds to seconds). This rapid measurement capability was critical to our application of automated measurement at closely spaced intervals down a long sediment core. No moving parts are in the spectrometer, and the instrument has almost no wavelength drift. For measurements performed during Leg 138, integration times were set to 2.6 s. Each spectrum measurement was performed three times and then averaged. Total measurement time for each sample, including moving the core, adjusting the sample-to-sensor distance, integrating the spectrum three times, and transmitting the data to the computer, was about 10 s.

A diode-array detector is affected by a thermal background signal. With the integration times we used, an increase in the detector's temperature of 1°C resulted in a 1% increase in the integrated counts, and a slight reduction of signal/noise ratios. A thermoelectric cooling device surrounding the detector reduced this background. To minimize costs, we used an inexpensive thermoelectric device from a picnic cooler. This device succeeded in reducing background levels in the detector, but was not adequate for a permanent installation. At the beginning of Leg 138, this device cooled the detector to 3°C, but after two months of nearly constant use, the device only reached 16°C. Temperature variability was gradual and changed by less than 2°C over a 24-hr period. Long-term (> 1 day) thermal drift effects were removed at sea. The small daily thermal drift of about 1% reflectance may be removed from the data during post-cruise processing, but this error is small enough (relative to the signals we observed) that one could ignore it in this application.

Computer Control and Data Processing System

All measurement functions were controlled by a 386-PC computer. Instrument control software was developed at Oregon State University, using the Microsoft Quickbasic language. Communications with the diode-array trigger and detector and with the stepper motor and limit switches in the core transport system used a data translation DT2801 12-bit analog and digital I/O board. Control of the sensor head servomotor used a low-cost data translation DT2811 12-bit analog and digital I/O board, plus a custom-made interface and drive circuit.

Because of the volume of data produced by this instrument (about 50 megabytes per day) and the need for data reduction at the same time as collection, all data were written by the 386-PC over ethernet, directly to a 600-megabyte disk controlled by a Sun SLC Unix workstation. We used Sun PCNFS software for this local network. All data processing was performed on the Unix workstation, and data archiving was performed using a QIC-150 tape drive on the workstation and on the *JOIDES Resolution* VAX computer system. The multiple computer strategy was successful, because it allowed the operator to process the data and examine the results almost as soon as they were collected.

Data Output, Calculations, and Standardization

To calculate the percentage reflectance of a sample, we must know the spectrum of the light source reflected from a perfect diffuse reflector (we refer to this as "White") and the background spectrum of the same reflector in the absence of illumination (we refer to this as "Black"). Reflected light from a sample as a function of wavelength (λ), $C(\lambda)$, illuminated in the same way as the standard, yields light intensities at the detector intermediate between "Black" and "White." The percentage reflectance (R) as a function of wavelength (λ) is given by:

$$R(\lambda) = 100 [C(\lambda) - \text{Black}(\lambda)] / [\text{White}(\lambda) - \text{Black}(\lambda)] \quad (1)$$

An example of this calculation is given in Figure 3.

The White (λ) reference values were measured by illuminating a block of Spectralon™ white reflectance standard in the same way as a sample. This material reflects better than 99.9% of incident light in the visible and near-infrared bands measured here. The material can be machined, sanded, or washed with soap (not detergent, which may leave residues that fluoresce) and water, and does not absorb water. In this study, the white standard block was wiped clean regularly with distilled water and a laboratory wipe and then air dried before using. The Black (λ) reference value was measured with the shutter closed on the light source. This gave the background light intensity, which we assumed was constant during the following measurements.

Both the White (λ) and Black (λ) standards were measured before each core section was analyzed. Noise in the calibration standards may have occurred as a result of human error when closing the shutter,

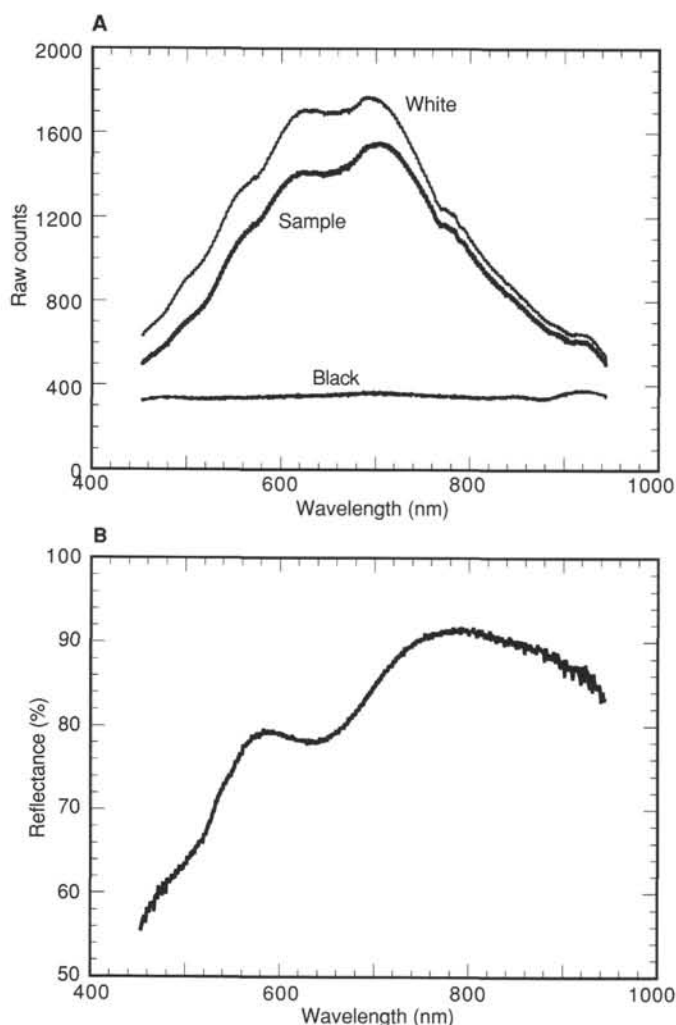


Figure 3. An example of the transformation of raw data to percentages of reflectance. **A.** Raw counts of light intensity measured at the diode array detector as a function of wavelength for "White" reference material, "Black" background, and one sample (138-851B-34X-2, 114 cm). **B.** Percentage of reflectance of the same sample after processing the raw count data using Equation 1.

of variations in ambient light, and of accidental tilting of the Spectralon block, which was mounted on a moving core boat. To minimize this noise in the calibration, the White (λ) and Black (λ) standards were averaged over ~ 12 -hr periods. Averaging did not combine measurements from different source lamps, as different lamps may have had different outputs.

RESULTS

Color reflectance spectra were measured in all sites of Leg 138. All cores were gently scrapped across their surface with a glass slide to expose a fresh, unsmear surface before being analyzed. Cores were analyzed while wet, shortly after splitting. The presence of water affects reflectance. Water effects are relatively small in the wavelengths we studied, but are large in discrete absorption bands at wavelengths >1400 nm (Gaffey, 1986; Clark, 1981). This is one reason our studies were limited to shorter wavelengths. Sample intervals ranged from 1 to 8 cm, depending on the scientific goals and time constraints at each site. The standard sample interval used at most sites was 4 cm. The color reflectance instrument producing roughly 1 Gb of data for the entire leg. With this amount of data, only initial processing was performed on board the ship. Our intent in this section is to point out some interesting features in the data and to outline potential applications of the data set. Because of shipboard time constraints and the need to compare to "ground truth" lithologic data in some of the same samples, any discussion of the results at present is preliminary. At sea, we limited ourselves to analyzing three band averages of downhole data, 450–500 nm (blue), 650–700 nm (red), and 850–900 nm (near infrared), and to plotting example spectra of lithologic types. Five examples of the output are shown here. First, we plot these three color channels downhole to give a large-scale view of sediment variability (Fig. 4). Second, we show the effects of sedimentary oxidation state superimposed on lithologic change (Fig. 5). Third, we search for color end members related to lithologies (Figs. 6 and 7). Fourth, we illustrate the use of color data for assembling composite depth sections from multiple holes (Fig. 8). Fifth, we compare these color data to other nonintrusive data sets and discuss the potential for use of these multiparameter data for high-resolution paleoceanographic studies of time series (Fig. 9).

A Lithologic Column in Color

At each site, the standard lithologic description for Leg 138 includes a downhole plot of reflectance in the blue, red, and near-infrared channels and example spectra from each lithologic unit. The column from Hole 845A (Fig. 4) exhibits relatively low reflectance (10%–30%) in the upper 135 mbsf and high reflectance (50%–80%) in the deeper section. To the first order, this brightness is a function of calcite concentration at this site (from nannofossil and foraminifer contents), which was low in the upper section and high in the lower section (see "Site 845" chapter, this volume). This result is not surprising. The reflectance spectrum of reagent-grade calcite is relatively flat and $>95\%$ at wavelengths from 500 to 1100 nm (Gaffey, 1984).

Additional information is contained within the reflectance spectra. Diatom ooze and siliceous clay in the upper section (Unit I) of Hole 845A are relatively dark, especially in the visible bands (<700 nm). This material has slightly higher reflectance in the near-infrared band (>700 nm) than in the visible bands (Fig. 4). A reflectance minimum is common in the red (650–700 nm) band, and this results in a greenish-gray or olive hue (commonly 5GY or 5Y in Munsell color codes) in this lithology. At present, we do not know if this reflectance spectrum results from the presence of biogenic silica or from trace components that co-occur with the siliceous sediments. For example, organic matter typically has low visible reflectance and high near-infrared reflectance (Hoffer, 1984), so it is possible that trace organic

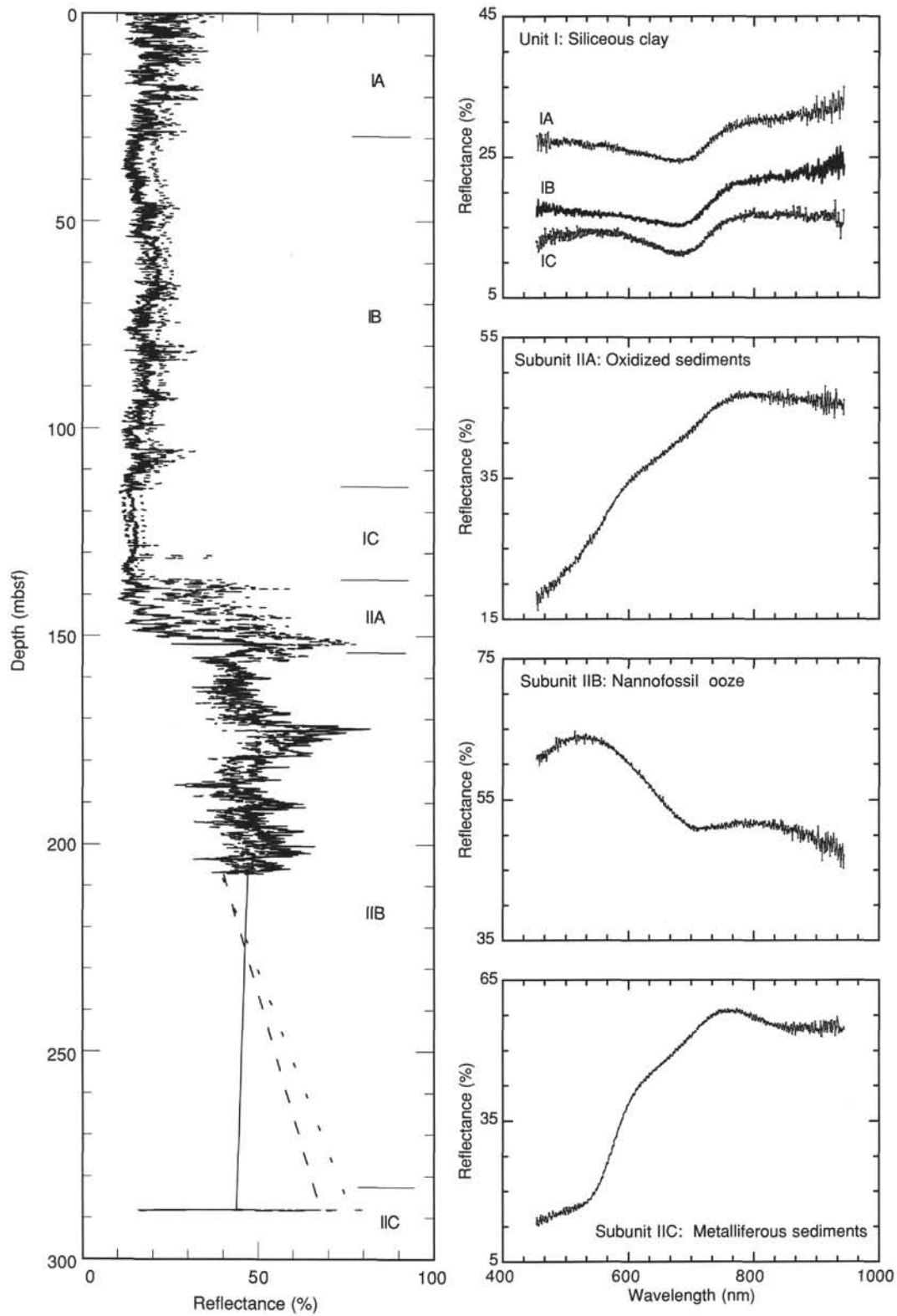


Figure 4. Downhole reflectance from Hole 845A showing three bands of reflectance data (blue = solid, red = dashed, and near-infrared = dotted). Examples of full spectra from each lithologic unit are shown at right.

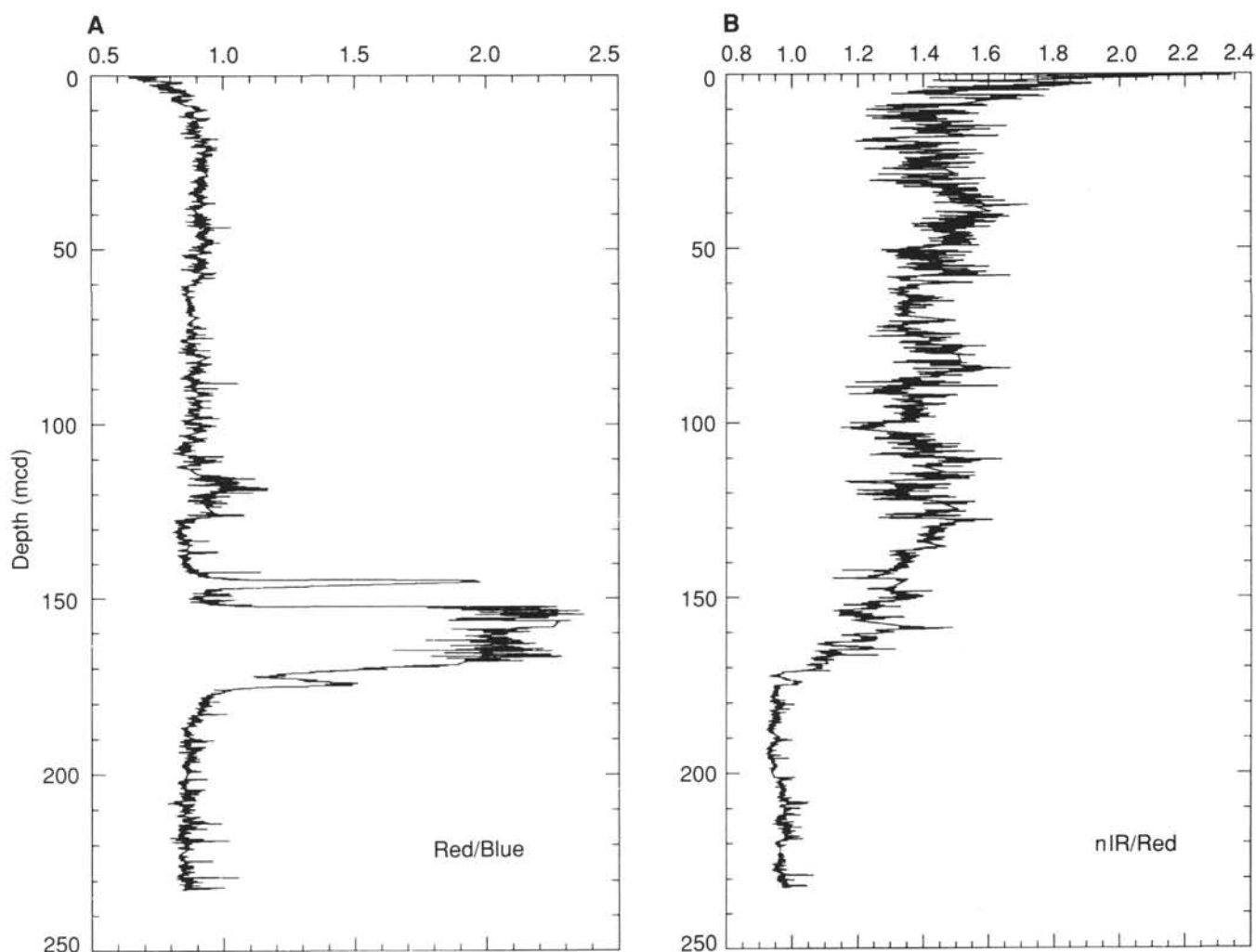


Figure 5. Red/Blue (A) and nIR/Red (B) ratios from Hole 845A plotted on the composite depth scale. These ratios vary independently of each other and respond to different sedimentary processes.

matter or pigments might affect the color spectrum significantly, despite low concentrations.

Calcite-rich sediments (nannofossil and foraminifer oozes) that we analyzed during Leg 138 often have a reflectance maximum in the lower visible bands (450–550 nm) and have somewhat lower reflectance in near-infrared bands. This gives the sediment a light bluish-gray hue. This pattern appears related to traces of diagenetic sulfide minerals, such as iron pyrite, in the carbonate-rich units (Subunit IIB) of Site 845 (Fig. 4). Pyrite commonly forms medium gray diagenetic bands that crosscut bedding and burrow structures.

The presence of oxyhydroxides in the sediments induces strong color changes. Iron oxyhydroxides, such as hematite and goethite, are highly reflective in the red (650–700 nm) and near-infrared (>700 nm) bands. Even minor concentrations of these oxyhydroxides change the color spectrum dramatically. The presence of oxyhydroxides may result from the presence of oxygen near the sediment/water interface (the brown–green transition, Lyle, 1983), from the presence of excess hydrogenous iron and manganese in low sedimentation-rate areas, or from hydrothermal influx near oceanic ridge crests or near basaltic basement (Heath and Dymond, 1977).

An interval of oxidized sediment containing hematite and goethite occurs in Hole 845A from 131 to 153 mbsf (Subunit IIA) and has a biostratigraphic age of 9–10 Ma (Fig. 4). In Site 845, this oxyhydroxide-

rich zone masked a transition from clayey diatom ooze (above) to diatom nannofossil ooze (below). In this zone, reflectance is highest in the near-infrared bands and also is relatively high in the upper visible bands (550–700 nm, yellow-orange-red). In part, this oxidized zone may result from low sedimentation rates in this interval (12–16 m/m.y.), but other intervals at this site had similar low sedimentation rates and did not contain oxyhydroxides. An alternate hypothesis is that anomalously high hydrothermal influx of iron and manganese may have occurred at this time, perhaps associated with a ridge crest jump at about this time in the eastern Pacific (Lyle et al., 1987). Metaliferous sediments in the basal section (Subunit IIC), near the contact with basalt, are rich in oxidized metals (such as iron and manganese) and appear red. This zone is more reflective in the upper visible and near-infrared bands than in the lower visible bands. (Fig. 4).

Isolating Lithologic Components of Color: A First Attempt

The presence of strong color signals associated with minor amounts of oxyhydroxides or sulfides masks the underlying color changes in the major lithologic components, such as calcite and biogenic opal. One might be able to see through the redox effects to examine the underlying variations of major lithologies. As a first attempt to isolate

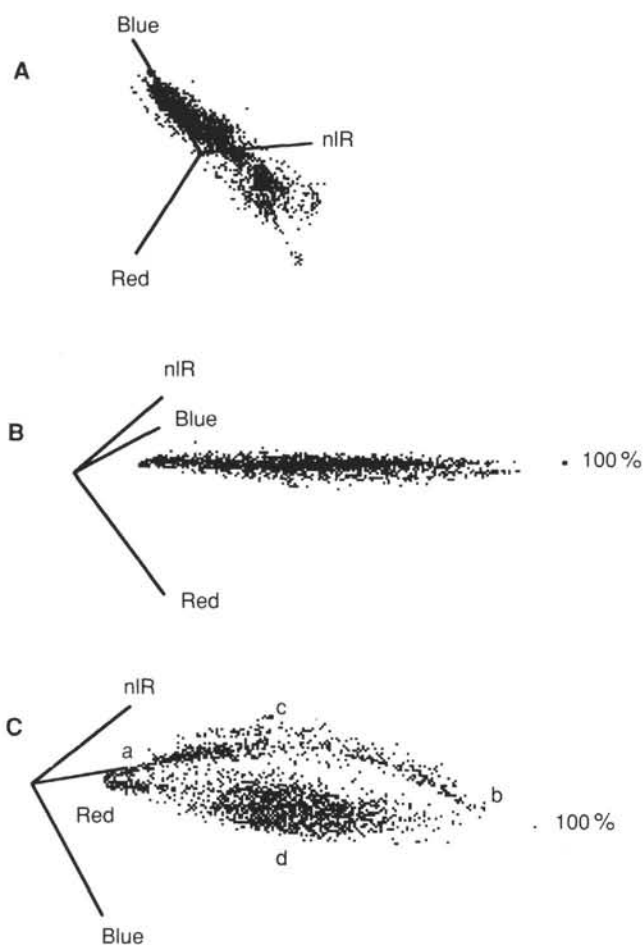


Figure 6. Three-dimensional plots of Blue-Red-nIR from all sites. Three projections are shown (A) end view, showing the minor axis of variability; (B) side view, showing the axis of least variability; and (C) Top view, showing the major axis of variability (from points "a" to "b"), and the minor axis of variability (from points "c" to "d"). The intersection of the axes marks the point of zero percentage of reflectance. The point of 100% reflectance has been labeled.

these effects, we examined ratios of spectral bands at Site 845. The ratio of red/blue reflectance is highly sensitive to the presence of oxyhydroxides or sulfides. Red/blue ratios >1.5 characterize the oxidized zone in the middle of Site 845. In the sulfide-bearing zone, this ratio is low and varies little (0.9 to 1.0), whether the sediments are composed of diatom ooze (the upper section) or of nannofossil ooze (the lower section; Fig. 5A). The ratio near-infrared (nIR)/red appears to reflect the change in lithologic character from nannofossil ooze in the lower section (nIR/red <1.1) to diatom ooze in the upper section (nIR/red >1.1 ; Fig. 5B), with no masking effect associated with the oxidized zone. Note that the transition from carbonate to siliceous sediments occurs within the oxidized zone.

Color Reflectance End Members

To explore the total range of variation in the color spectra measured during Leg 138, we plotted the three bands, blue (450–500 nm), red (650–700 nm), and nIR (850–900 nm), in three-dimensional space, using DataDeskTM software with shipboard Macintosh computers. We rotated the axes to view different aspects of spectral variability in these three bands. The data were first decimated to include about 200 samples spread evenly throughout the sedimentary column from each of the 11 drill sites (844–854). The three projections presented in

Figures 6A through 6C show that the reflectance values from the blue, red, and near-infrared bands form a nearly planar surface. The planar structure is best seen by comparing Figure 6B, which views the thin edge of the plane with a ratio of nIR/red of about 1.4, with Figure 6C, which shows the flat surface of the plane. Points on the plane form arcuate mixing zones between the low- and high-reflectance extremes (Fig. 6C). A labeled symbol identifies the point where reflectance in all three bands should be 100%.

The major axis of variability falls approximately along this line and can be described as "brightness" (the average reflectance). The "dark" extreme (labeled "a" in Fig. 6C) has about 10% reflectance in the blue and red bands and about 15% reflectance in the near-infrared band. The "bright" (labeled "b" in Fig. 6C) extreme has reflectance of about 85% in the blue, 95% in the red, and 90% in the nIR bands. Spectra of these extremes are shown in Figure 7 (left and right). The dark end member (Fig. 7, left) is characterized by Sample 138-854C-6H-7, 41 cm, which is black (Munsell 10YR 2/2), clayey, metaliferous sediment. The pale end member (right) is white (Munsell N8) nannofossil ooze (Sample 138-848C-8H-5, 58 cm). It appears that differences in position along the major axis are primarily a function of calcium carbonate content.

The minor axis of variability on the plane (Fig. 6C) separates an arcuate limb having higher reflectance in the nIR and red bands (upper zone in Fig. 6C) from those having higher reflectance in the blue band (lower zone in Fig. 6C). Spectra from the extreme points of the minor axis are shown in Figure 7 (top and bottom). The upper extreme (labeled "c" in Fig. 6C) has 30% blue, 50% red, and 70% nIR reflectance and is pale brown (Munsell 10YR 7/4), clayey, radiolarian nannofossil ooze that contains manganese and iron oxyhydroxides (Sample 138-852C-12H-2, 110 cm). The lower extreme (labeled "d" in Fig. 6C) has 65% blue, 55% red, and 50% nIR reflectance. This sample is composed of light greenish-gray (Munsell 5GY 7/1) diatom, foraminifer, radiolarian nannofossil ooze (Sample 138-848C-3H-3, 98 cm). Sediments on this lower limb lack oxyhydroxides and frequently contain sulfides. Thus, the minor axis can be described as an oxidation/reduction effect. A zone is found between these two extremes that contains few samples, which suggests that intermediate samples containing both oxyhydroxides and sulfides are uncommon. This is consistent with visual observations that transitions from brown (oxidized) to green (reduced) sediments are generally abrupt. Intermediate states were not observed.

This three-dimensional view of color variability is incomplete, because it examines only three 50-nm-wide color bands extracted from the 511 channels measured. However, this simple analysis demonstrates that multiple processes contribute to color variability in marine sediments and that it may be possible to extract information about these processes from color reflectance data. Further work may reveal other patterns of variability in the data set. At present, we do not know whether each lithologic component has a unique color spectrum or whether color spectra may be treated as linear combinations of different end-member spectra related to lithology. Each indicator responds to different sedimentological processes.

Assembling Composite Depth Sections

Color reflectance data were used at sea, along with gamma-ray attenuation porosity evaluator (GRAPE) density and magnetic susceptibility data, to compare different holes at each site and to assemble composite depth sections (Hagelberg et al., this volume). Initial correlations were generally performed using GRAPE density or magnetic susceptibility, because these data were measured on unsplit cores and thus were available sooner than color data. Color was used primarily to check and modify hole-to-hole correlations based on other nonintrusive data sets. An example of hole-to-hole correlations, using red (650–700 nm) percentage reflectance data, GRAPE density, and magnetic susceptibility in Site 845 is presented in Figure 8. We

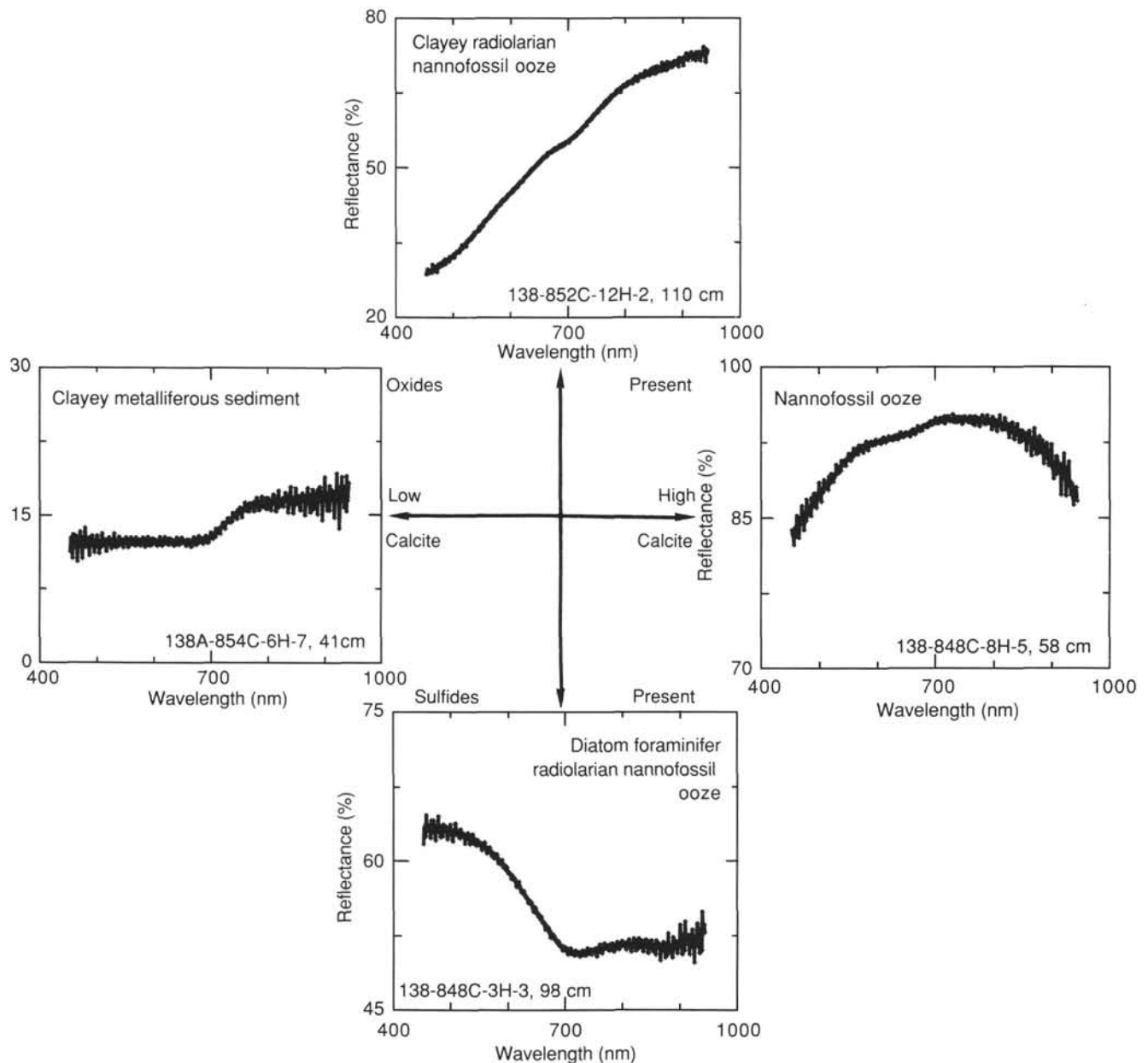


Figure 7. Spectra of end members from Figure 5 related to lithology. See text for details.

found it extremely valuable to have all three high-resolution data sets available for comparison of holes, as each illustrated different downhole structures, and thus added unique information to constrain correlations.

High-frequency Variability

Reflectance spectroscopy holds great promise for characterizing short-term variability of lithologies at a resolution greater than might be done with traditional discrete measurements. In Figure 9, we plot a time series of GRAPE density, which is closely linked to variations in percentage of CaCO_3 and percentage of reflectance in the red channel in Core 138-852B-2H. The data are plotted vs. age, based on linear interpolation among magnetostratigraphic datums at 0.73 Ma (Brunhes/Matuyama boundary) and 1.63 Ma (top of Olduvai event; Shackleton et al., this volume). The sedimentation rate in this interval is 13 m/m.y. Both time series have been interpolated to constant time intervals of 3000 yr (broader than the original sampling in depth) and

smoothed with a 9000-yr Gaussian filter so that they can be compared with the same resolution. The age model is preliminary, but serves to illustrate the scale of temporal variability recorded in these sediments.

While the grape and color time series are in some ways similar, they also have significant differences. Red reflectance appears to contain more variability at shorter periods than is present in the GRAPE data. This appearance is confirmed by power spectral analysis of these data, which suggests that over this interval the GRAPE data contains the Milankovitch periods of 100 and 41 k.y., and the color reflectance does not. This example shows that reflectance does not respond in lock step with carbonate, but adds additional information about processes contributing to the sedimentary record. In this example, possible influences on red reflectance could be variations in sedimentary redox conditions associated with organic carbon input, or variable input of clays from eolian transport. Although the cause of the color variability is not constrained based on shipboard data, this analysis allows us to pose hypotheses rapidly, and has set the stage for further analysis post-cruise.

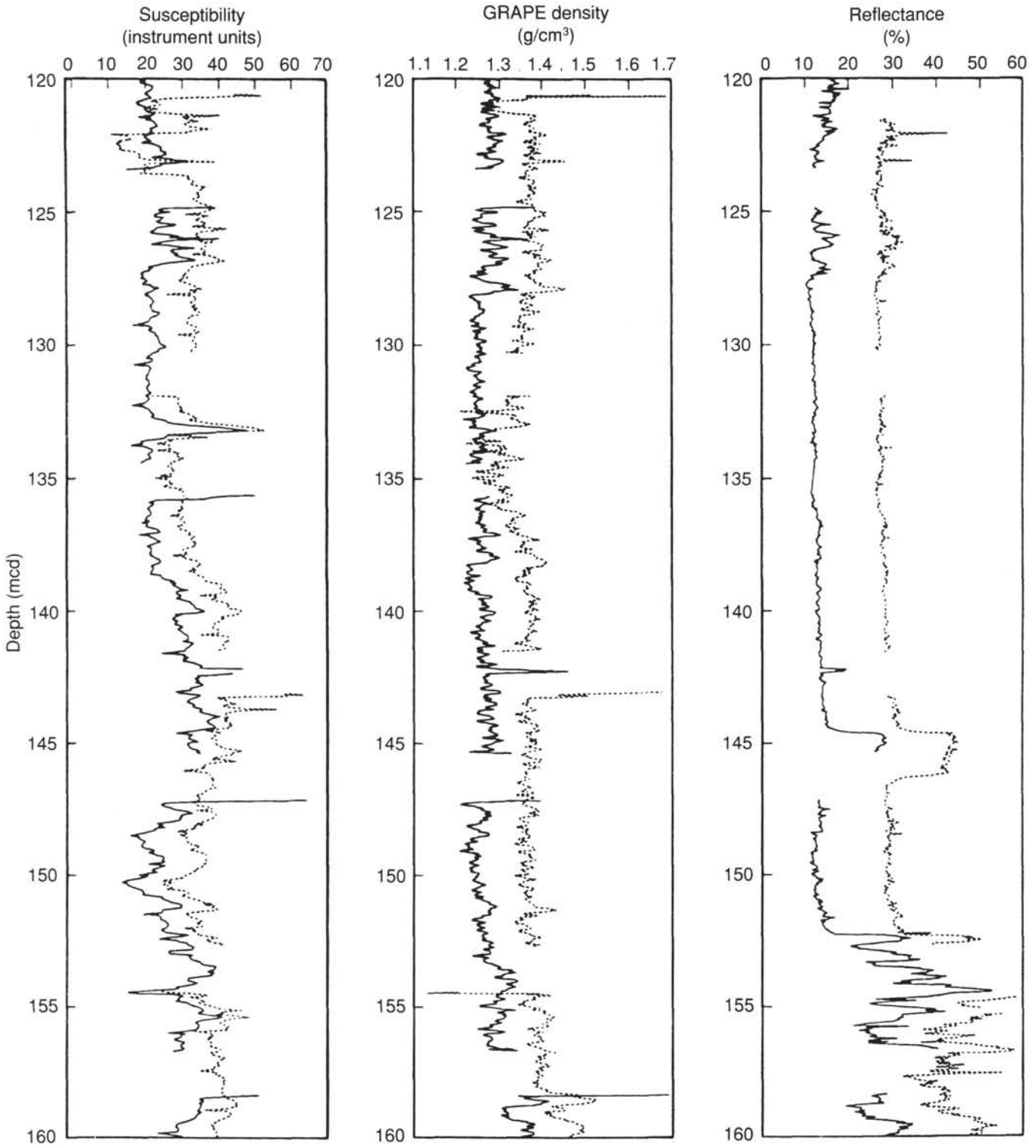


Figure 8. Example of hole-to-hole correlations using GRAPE, percentage of red reflectance, and magnetic susceptibility. Solid line = Hole 845B; dashed line = Hole 845C.

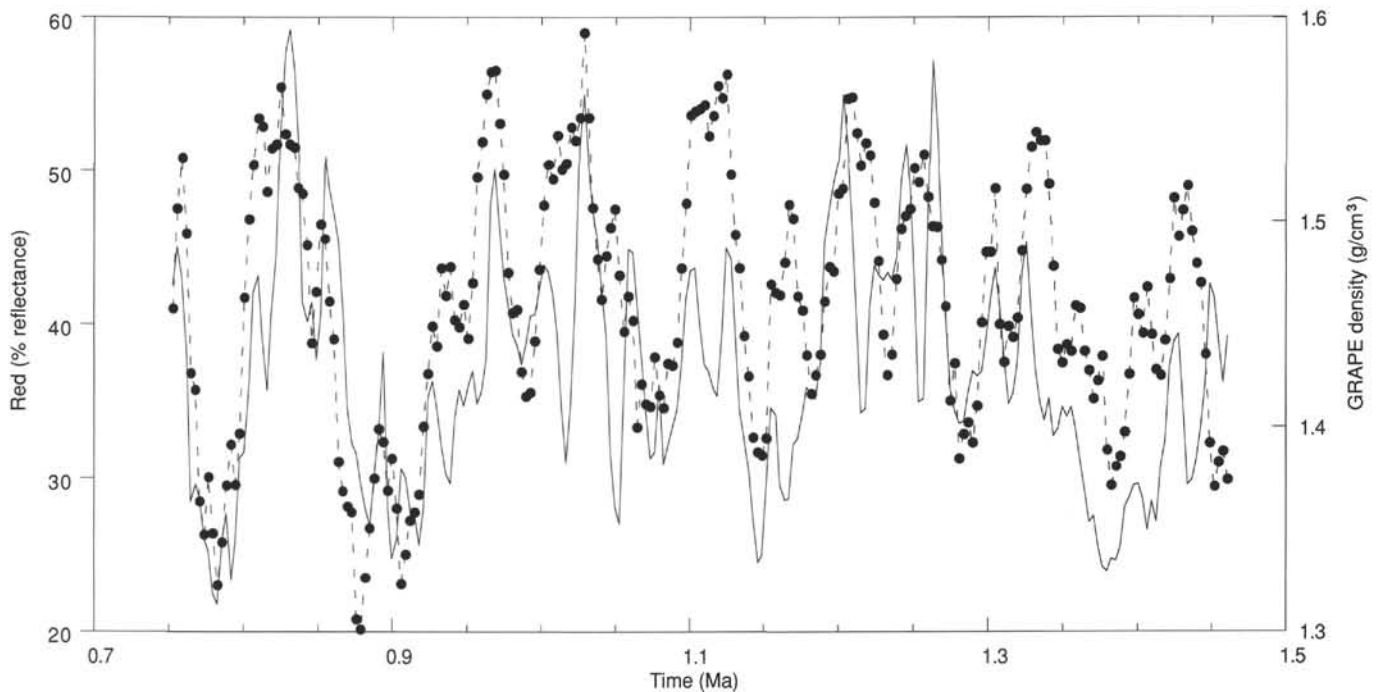


Figure 9. Time series of GRAPE (dashed line with solid dots) and percentage of red (650–700 nm) reflectance (solid line) in Core 138-852B-2H. Time control is from magnetic reversal stratigraphy (see “Site 852” chapter, this volume).

CONCLUSIONS

An experiment with color reflectance spectroscopy during Leg 138 was successfully completed, and this instrumentation proved to be reliable at sea. Although analysis of data has not yet been completed, initial results suggest that these data will permit rapid, noninvasive characterization of major lithologies and the oxidation state of sediments. At present, we are unclear how unique or linear are the relationships between color and lithology, and substantial work will be needed to provide ground-truth calibration of the color information. This method has great potential for providing lithologic data at much higher sampling densities than would be possible with traditional discrete samples.

A partial goal of this experiment was to evaluate how a split-core sensing system would affect core archiving during ODP cruises. The success of this experiment suggests that further developments in split-core sensing are warranted. Our experience with this prototype instrument yielded several recommendations:

1. The color reflectance instrument generally was not the rate-limiting step in core processing. Each core took 60 to 90 min. to analyze. This time could be cut in half by using a higher intensity light source.
2. When cores are split, they have unpredictable roughness and smearing of the surface because of wire or saw cutting. We attempted to alleviate this problem by scraping each section across the core with a glass slide. This was time consuming, but had the benefit of producing an integrated sample from each core section, which was used for X-ray fluorescence analysis during Leg 138. In the future, a more uniform, clean core-splitting process should be considered.
3. The shipboard environment is electrically and thermally noisy, dirty, and contains a lot of vibration. This caused some problems with short life span of source lamps (1–2 days) and presented difficulties for keeping calibration materials clean. While these problems were not serious enough to impede measurement, attention to these details should improve the reliability and speed of data acquisition.

4. It may be possible to add other instruments to characterize split cores. Examples are magnetic susceptibility, video imaging, far-infrared reflectance, and fluorescence.

5. Significant increases in computer power at sea are needed to handle the large quantities of data produced by these types of instruments. The present computer facilities on board *JOIDES Resolution* are not up to this task.

ACKNOWLEDGMENTS

We thank USSAC for funds that allowed us to develop this instrumentation. The project started at OSU as part of the NSF Research Experience for Undergraduates Program. We also thank ODP and *JOIDES Resolution* staff for accommodating this experiment during Leg 138 with reasonably good humor and OSU staff for assistance, notably P. Kalk and J. Wilson.

REFERENCES

- Barranco, F. T., Jr., Balsam, W. L., and Deaton, B. C., 1989. Quantitative reassessment of brick red lutites: evidence from reflectance spectrophotometry. *Mar. Geol.*, 89:299–314.
- Bearman, S., 1990. Exploiting distributed parallelism in multi-sensor systems. *Sci. Comput. Automat.*, January, 43–51.
- Chester, R., and Elderfield, H., 1966. The infra-red determination of total carbonate in marine carbonate sediments. *Chem. Geol.*, 1:277–290.
- Clark, R. N., 1981. The spectral reflectance of water-mineral mixtures at low temperatures. *J. Geophys. Res.*, 86:3074–3086.
- Gaffey, S. J., 1986. Spectral reflectance of carbonate minerals in the visible and near infra-red (0.35 to 2.55 microns): calcite, aragonite, and dolomite. *Am. Mineral.*, 71:151–162.
- Goetz, A.F.H., Rowan, L. C., and Kingston, M. J., 1982. Mineral identification from orbit: initial results from the shuttle multispectral infrared radiometer. *Science*, 218:1020–1024.
- Heath, G. R., and Dymond, J., 1977. Genesis and transformation of metal-liferous sediments from the East Pacific Rise, Baver Deep, and Central Basin, Northwest Nazca Plate. *Geol. Soc. Am. Bull.*, 88:723–733.

- Hoffer, R. M., 1984. Remote sensing to measure the distribution and structure of vegetation. In Woodwell, G. M. (Ed.), *The Role of Terrestrial Vegetation in the Global Carbon Cycle: Measurement by Remote Sensing*: New York (Wiley), 131–159.
- Hunt, G. R., 1977. Spectral signatures of particulate minerals in the visible and near infrared. *Geophysics*, 42:501–513.
- Lyle, M., 1983. The brown-green color transition in marine sediments: a marker of the Fe(III)-Fe(II) redox boundary. *Limnol. Oceanogr.*, 28:1026–1033.
- Lyle, M., Leinen, M., Owen, R. M., and Rea, D. K., 1987. Late Tertiary history of hydrothermal deposition at East Pacific Rise: correlation to volcano-tectonic events. *Geophys. Res. Lett.*, 14:595–598.

Ms 138A-104